DOI: 10.1002/chem.200500184

A Multisite Molecular Mechanism for Baeyer–Villiger Oxidations on Solid Catalysts Using Environmentally Friendly H_2O_2 as Oxidant

Mercedes Boronat,[a] Avelino Corma,*[a] Michael Renz,[a] Germán Sastre,[a] and Pedro M. Viruela[b]

Abstract: The molecular mechanism of the Baeyer–Villiger oxidation of cyclohexanone with hydrogen peroxide catalyzed by the Sn-beta zeolite has been investigated by combining molecular mechanics, quantum-chemical calculations, spectroscopic, and kinetic techniques. A theoretical study of the location of Sn in zeolite beta was performed by using atomistic force-field techniques to simulate the local environment of the active site. An interatomic potential for Sn/Si zeolites, which allows the simulation of zeolites containing Sn in a tetrahedral environment, has been developed by fitting it to the experimental properties of quartz and SnO_2(rutile). The tin active site has been modeled by means of a $Sn(OSiH_3)_3OH$ cluster, which includes a defect in the framework that provides the flexibility necessary for the interaction between the adsorbates and the Lewis acid center. Two possible reaction pathways have been considered in the computational study, one of them involving the activation of the cyclohexanone carbonyl group by Sn (1) and the other one involving hydrogen peroxide being activated through the formation of a tin–hydroperoxo intermediate (2). Both the quantum-chemical results and the kinetic study indicate that the reaction follows mechanism 1, and that the catalyst active site consists of two centers: the Lewis acid Sn atom to which cyclohexanone has to coordinate, and the oxygen atom of the Sn−OH group that interacts with H_2O_2 forming a hydrogen bond.

Keywords: Baeyer–Villiger reactions · density functional calculations · kinetics · Lewis acids · tin · zeolites

Introduction

Heterogeneous catalysis is one of the disciplines that has introduced numerous breakthroughs in the field of chemical reactivity. This is reflected in the large number of industrial processes that are based on solid catalysts. Until recently, most of the advances were made on the basis of chemical intuition and analogies. However, it is becoming generally accepted that major breakthroughs in the field of heterogeneous catalysis will come through a better understanding of the catalytic mechanisms at a molecular level. To do this, we can combine well-defined catalyst synthesis methods, in situ characterization techniques, powerful quantum-chemical calculations, and kinetic experiments. We will show here that by applying this multidisciplinary approach we are able to propose a molecular mechanism for Baeyer–Villiger oxidations on a solid catalyst using H_2O_2 as the oxidant.

The Baeyer–Villiger reaction involves the oxidation of a ketone to an ester or lactone [Eq. (1)].[1]

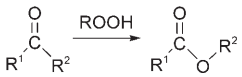

(1)

Peracids like trifluoroperacetic acid, perbenzoic acid, and *m*-chloroperbenzoic acid have been traditionally used as oxidants in the Baeyer–Villiger reaction. However, they show important disadvantages such as the lack of selectivity due to the ability of the peracids to oxidize other functional groups, the production of large amounts of carboxylic acid waste which has to be recycled and can catalyze undesired side reactions, and safety issues.[1b–d] For these reasons, attempts have been made to replace peracids by hydrogen

[a] Dr. M. Boronat, Prof. Dr. A. Corma, Dr. M. Renz, Dr. G. Sastre
Instituto de Tecnología Química, UPV-CSIC
Universidad Politécnica de Valencia, Av. de los Naranjos
s/n, 46022 Valencia (Spain)
Fax: (+34) 963-877-809
E-mail: acorma@itq.upv.es

[b] Prof. Dr. P. M. Viruela
Institut de Ciència Molecular, Universitat de Valencia
C/Dr. Moliner 50, 46100 Burjassot (Spain)

Supporting information for this article is available on the WWW under http://www.chemeurj.org/ or from the author.

peroxide which is commercially available, easy to handle, and only generates water as a side product. Pt-, Zr-, Re-, Se-, As-, and Mo-based[2] homogeneous as well as solid catalysts[3] have been reported to activate hydrogen peroxide for Baeyer–Villiger oxidations. Recently, Corma et al.[4] showed that Sn-beta, with Sn tetrahedrally coordinated in the zeolite framework, is highly active and selective for the Baeyer–Villiger oxidation of several ketones and aldehydes with hydrogen peroxide. To explain the high chemoselectivity observed, it was proposed that the catalyst does not activate hydrogen peroxide but instead activates the carbonyl group of the ketone or aldehyde making this more reactive towards H_2O_2 attack.

The classical Baeyer–Villiger mechanism involves two steps (see Scheme 1): 1) addition of the peracid to the ketone to form a tetrahedral adduct known as the Criegee intermediate and 2) concerted rearrangement of the Criegee intermediate to give the ester or lactone product and a carboxylic acid. The second step, that is, the migration step, is usually rate-determining, but depending on the reaction conditions and the organic reactant, addition can become in some cases the rate-determining step. When hydrogen peroxide is used as the oxidant, water is obtained as a product instead of an acid, but the reaction is supposed to proceed through the same mechanism.

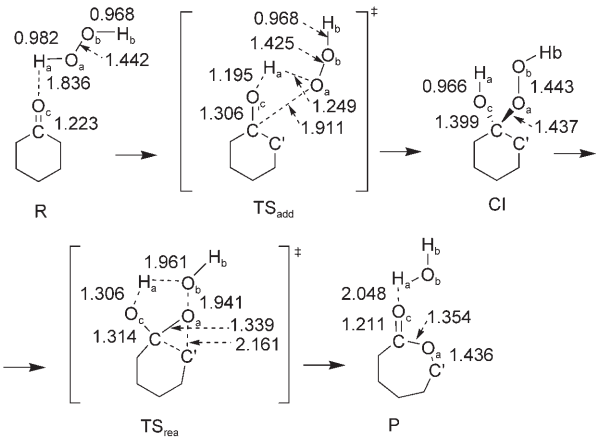

Scheme 1. Structures involved in the noncatalyzed Baeyer–Villiger reaction mechanism.

Theoretical studies on the mechanism of Baeyer–Villiger oxidations of ketones and aldehydes with peracids and hydrogen peroxide in the homogeneous phase[5] have been presented that take into account acid catalysis as well as substituent and solvent effects. With respect to metal catalysis, only two computational studies on the mechanism of Ti and Sn-catalyzed Baeyer–Villiger oxidations of ketone with hydrogen peroxide have been reported in the literature.[6] In these papers, the catalytic active site was modeled with small $Ti(OH)_4$ or $Sn(OH)_4$ unconstrained clusters, which are useful to investigate general reactivity trends but cannot reproduce the behavior of real metal-containing molecular-sieve catalysts. In particular, it has been recently shown[7] that the stability of certain reaction intermediates is marked by the local environment of the zeolite active site. Nevertheless, through detailed theoretical mechanistic work, the authors concluded that there are two pathways for the formation of the Criegee intermediate, one of which begins with the formation of a tin–hydroperoxo species. They also concluded that a mechanism in which tin activates the ketone carbonyl group cannot explain the rate enhancements achieved with tin-containing redox molecular-sieve catalysts. Because in our case we were not able to identify by different spectroscopic methods the formation of tin hydroperoxide and yet, on the contrary, we observed the interaction of the carbonyl group with the Sn atoms in Sn-beta zeolite,[4] we decided to perform a detailed mechanistic study of the Baeyer–Villiger reaction using H_2O_2 as the oxidant. Thus, in the present work, the mechanism of the Baeyer–Villiger oxidation of cyclohexanone with hydrogen peroxide catalyzed by Sn-beta zeolite has been studied by using computational methods and experimental kinetics based on the absolute rate theory. Two possible reaction pathways have been considered: the classical one involving activation of the hydrogen peroxide and formation of a tin–hydroperoxo intermediate that will attack the ketone carbonyl group, and an alternative mechanism in which tin activates the carbonyl group of the ketone, making it more reactive towards H_2O_2 attack. Both the theoretical calculations and the experimental kinetic study indicate that the reaction mechanism requires two close sites and involves activation of the cyclohexanone carbonyl group by the Sn atom and weak bonding of H_2O_2 onto a Sn–OH group, but not the formation of a tin–hydroperoxo intermediate.

Results and Discussion

Noncatalyzed reaction mechanism: The structures involved in the mechanism of the gas-phase or noncatalyzed Baeyer–Villiger oxidation of cyclohexanone with hydrogen peroxide are shown in Scheme 1, together with the optimized values of their most important geometric parameters. Initially, cyclohexanone and hydrogen peroxide form a hydrogen-bound complex R which is 7.1 kcal mol^{-1} more stable than the separated reactants. Then, through transition state TS$_{add}$, the H_a and O_a atoms of H_2O_2 add to the oxygen and carbon atoms of the carbonyl group, respectively, breaking the H_a–O_a bond and yielding the Criegee intermediate (CI), which is 4.4 kcal mol^{-1} more stable than R. The C–O_a and C–O_c distances in this structure correspond to single bonds, and the C atom is tetrahedrally coordinated. The activation energy for the addition step, calculated as the energy difference between TS$_{add}$ and R, is high (31.6 kcal mol^{-1}) because all the bond breaking and formation occurs through a strained four-membered ring. In a second step, and in a concerted manner, the O_a–O_b bond breaks, the O_a atom is inserted into the C–C′ bond, the H_a atom moves towards O_b, and the carbonyl group is regenerated. The activation energy calculated as the energy difference between TS$_{rea}$ and CI is

42.9 kcal mol^{-1}, indicating that this is the rate-determining step. This process is irreversible and yields a complex between ε-caprolactone and a water molecule (P) that is 58.4 kcal mol^{-1} more stable than R. The geometries and energies obtained are similar to those previously reported for the reaction of acetone and hydrogen peroxide,[5d,6b] and in agreement with the experimental observation that Baeyer–Villiger oxidation of ketones with H_2O_2 needs catalytic activation to occur.

Selection of the Sn-beta active-site model by the adsorption study of reactants and products: In order to better understand the nature of the interaction between the tin active site and the substrates and products (adsorption constants and heats of adsorption), and choose an appropriate model to describe the reaction mechanism, we initially studied the adsorption of water (WA), hydrogen peroxide (HP), cyclohexanone (CH), and ε-caprolactone (LA) on the three cluster models described in the Experimental Section. It can be seen in Table 1 that adsorption energies on cluster A are considerably smaller than those on clusters A′ and B, and that the optimized Sn–$O_{adsorbate}$ distances in the rigid model are between 0.3 and 0.7 Å longer than in the more flexible systems. The reason for this is that the Sn-beta catalyst is a Lewis acid that tends to accept electron density from the Lewis base molecules present in the reaction medium. The most important donor–acceptor interaction occurs between the HOMO of the dissolved molecule, which is in all cases the lone pair or p_z orbital on the oxygen atom, and the LUMO of the catalyst, which is a combination of the four $\sigma^*_{Sn\text{-}O}$ antibonding orbitals. This interaction implies a lengthening of the four Sn–$O_{framework}$ distances that is more difficult in the rigid cluster model, this being the reason for the low adsorption energies and long Sn–$O_{adsorbate}$ distances obtained with cluster A.

Table 1. Adsorption energies [kcal mol^{-1}], Sn–$O_{adsorbate}$ distances [Å], and CO vibrational frequency shifts [cm^{-1}] calculated for water (WA), hydrogen peroxide (HP), cyclohexanone (CH), and ε-caprolactone (LA) adsorbed onto the different cluster models used in this work. All shifts are scaled by the factor 0.9573 as recommended in reference [8].

	Cluster	WA	HP	CH	LA
E_{ads}	A	−3.9	−5.3	−1.6	−6.6
	A′	−12.9	−11.6	−10.0	−14.1
	B	−13.9	−12.4	−9.7	−14.5
			(−6.6)[a]		
	B-w	−7.9	−8.9	−4.9	−10.4
		(−14.1)[a]	(−14.0)[a]		
rSn–$O_{adsorbate}$	A	2.599	2.858	2.889	3.059
	A′	2.304	2.368	2.290	2.316
	B	2.302	2.363	2.431	2.472
	B-w	2.239	2.314	2.218	2.228
$\Delta\tilde{\nu}_{CO}$	A			−26.6	−27.5
	A′			−63.5	−102.7
	B			−62.0	−84.6
	B-w			−75.6	−107.8

[a] Coordinated to O_5 through a hydrogen bond.

In the case of cyclohexanone and ε-caprolactone, there is a second donor–acceptor interaction between the HOMO of the catalyst, which is a combination of the lone pairs on the oxygen atoms of the cluster, and the LUMO of the organic molecule, which is the antibonding π^*_{CO} on the carbonyl group. This interaction weakens the CO double bond, and as a result the CO bond length increases and the $\tilde{\nu}_{CO}$ vibration frequency is shifted to smaller values. The calculated shifts of the $\tilde{\nu}_{CO}$ vibrational frequencies obtained for model B agree well with the experimental values of −48 and −70 cm^{-1} that we observed in the IR spectra of cyclohexanone and ε-caprolactone adsorbed on Sn-beta. The results obtained with model A′ are slightly worse for the lactone, while model A provides $\Delta\tilde{\nu}_{CO}$ values that are too small. It can therefore be concluded that a certain degree of flexibility in the structure of the framework Sn site is necessary to allow the interaction between the dissolved molecules and the tin center to occur. Model A′, in which one -$OSiH_3$ group is set completely free in the geometry optimizations, is not real because the zeolite framework does no allow such deformations. Therefore, model B, which represents a catalyst in which one of the Sn–O–Si bonds has been hydrolyzed, was used to study the zeolite-catalyzed reaction mechanisms.

Model B has further consequences for the reaction mechanism. For the IR experiment and the adsorption study presented in this section, only one reaction center and one substrate molecule have been considered. However, in the next sections it is shown that in the presence of molecules that are prone to hydrogen bonding (WA and HP), these types of hydrogen bonds are formed with the oxygen atom of the Sn–OH group. Consequently, the Sn-beta catalyst active site has to be considered as bifunctional, and adsorption energies should be considered for a pair of substrates: one acting as Lewis base coordinated to the Sn center and the second one responsible for the hydrogen bonding of H_2O_2 on the oxygen of the Sn–OH group, that in turn significantly influences the coordination of Sn.

Sn-beta-catalyzed reaction mechanisms

Mechanism 1: According to this mechanism (Scheme 2), tin activates the carbonyl group of adsorbed cyclohexanone making it more reactive towards the attack of hydrogen peroxide. The optimized values of the most important geometric parameters of the structures involved are summarized in Table 2, and the calculated energy profile is depicted in Figure 1a. In the first step, both CH and HP are adsorbed onto the active site forming the reactants complex R1. It is to be noted that in this structure the O_c atom of the CH carbonyl group coordinates to the Sn atom, with a resulting Sn–O_c distance of only 2.2 Å, while HP does not directly interact with tin but forms a hydrogen bond with the O_5 atom of the zeolite catalyst. The relative orientation of CH and HP in structure R1 is very favorable for the addition step, the dis-

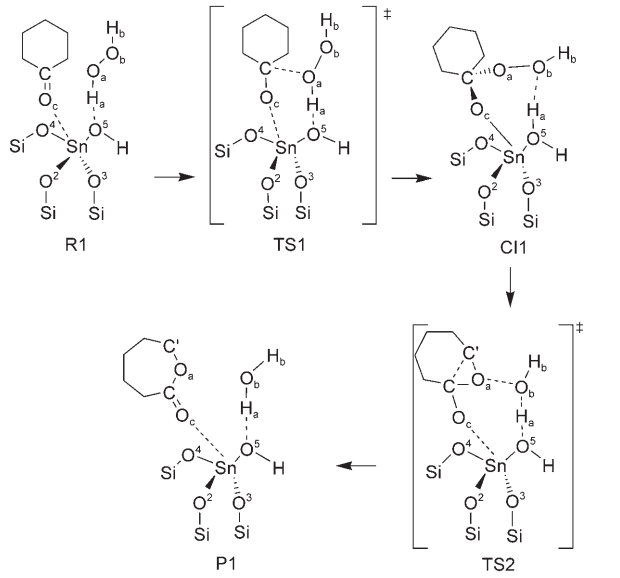

Scheme 2. Structures involved in the Sn-beta-catalyzed Baeyer–Villiger reaction mechanism 1.

Table 2. Optimized values of the most important distances [Å] of the structures involved in mechanism 1. The atom labeling is shown in Scheme 2.

	R1	TS1	CI1	TS2	P1
rSn–O_c	2.210	2.060	1.940	2.037	2.221
$r$$O_c$–C	1.240	1.300	1.400	1.327	1.238
rC–O_a	2.824	1.783	1.438	1.340	1.312
$r$$O_a$–$O_b$	1.440	1.431	1.459	1.804	3.144
$r$$O_a$–$H_a$	0.991	1.166	1.977[a]	1.149[a]	0.980[a]
$r$$O_5$–$H_a$	1.703	1.228	0.979	1.253	1.773
rSn–O_5	1.947	2.031	2.389	2.028	1.938

[a] Distance $r$$O_b$–$H_a$.

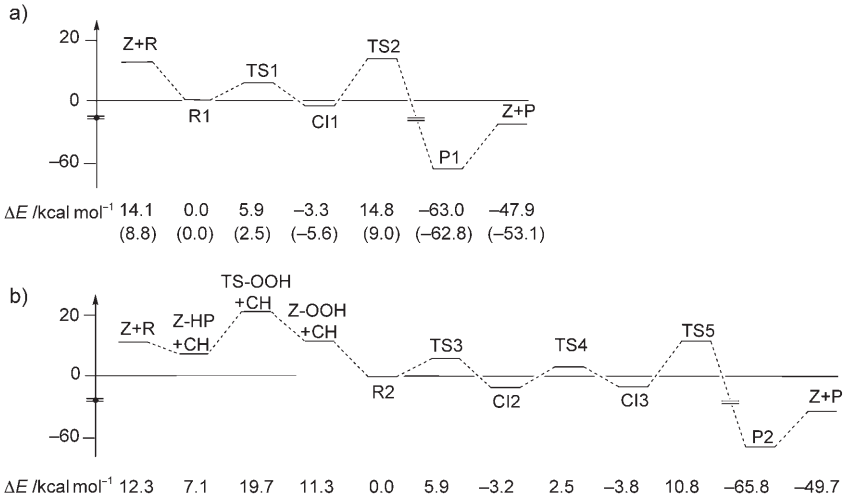

Figure 1. Calculated energy profiles for the Sn-beta-catalyzed reaction mechanisms 1 and 2 (a and b, respectively). The values in brackets for mechanism 1 have been obtained with model B-w.

tance between O_a and the C atom of the carbonyl group being only 2.8 Å. In the transition state TS1, the carbonyl double bond weakens and the interaction between O_c and the Sn atom increases. The H_a atom is transferred from the hydrogen peroxide to O_5, and a bond is formed between the carbonyl C atom and O_a, yielding the Criegee intermediate CI1. The activation energy for this concerted process, calculated as the energy difference between TS1 and R1, is low (5.9 kcal mol^{-1}) because all the bond breaking and bond formation occurs through a 6-membered ring. In the Criegee intermediate CI1 there is a single bond between O_c and the tin center and quite a strong hydrogen bond between O_b and H_a, and the structure is 3.3 kcal mol^{-1} more stable than R1.

In the second reaction step, that is, the rearrangement step, the Sn–O_c bond weakens and the carbonyl double bond is regenerated. At the same time, the O_a oxygen atom is inserted into the C–C′ bond, the O_a–O_b bond is broken, and the H_a hydrogen atom is transferred from O_5 to O_b, resulting in the formation of a water molecule. The whole process occurs in a concerted manner through transition state TS2, with an activation barrier with respect to CI1 of 18.1 kcal mol^{-1}. The reaction product P1 is a molecule of ε-caprolactone coordinated to the tin center and a water molecule forming a hydrogen bond with the O_5 atom of the catalyst model. The reaction energy, calculated as the energy difference between P1 and R1, is similar to that obtained for the noncatalyzed process (ca. −60 kcal mol^{-1}).

The Baeyer–Villiger oxidation of acetone with hydrogen peroxide was theoretically studied by Sever and Root[6b] by using a $Sn(OH)_4$ cluster to simulate the tin active site. They proposed a reaction path with an addition step similar to that obtained in this work, although their calculated activation barrier was higher, 11.1 kcal mol^{-1}. However, they considered that in the rearrangement step, the O_b–H_b fragment is transferred from the hydrogen peroxide to the tin center, and that another Sn–O bond has to be broken to yield a water molecule as a product. This process is clearly less favorable energetically than the reaction path proposed in our work.

Mechanism 2: The initial step in mechanism 2 (see Figure 1b and Scheme 3), is the formation of a tin–hydroperoxo species (Z-OOH) from adsorbed hydrogen peroxide (Z-HP) through transition state TS-OOH. HP coordinates to the active site both by interaction of the lone pair of O_a with the empty σ^*_{Sn-O} antibonding orbitals and by one hydrogen bond between H_b and the O_4 atom of the cluster. Then, through

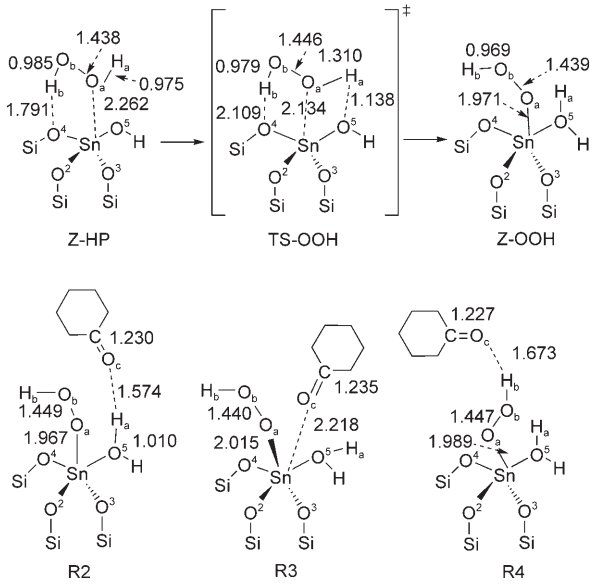

Scheme 3. Optimized geometries of the structures involved in the mechanism of tin–hydroperoxo intermediate formation (top) and of the three complexes obtained by adsorption of cyclohexanone on this tin–hydroperoxo intermediate (bottom). Distances in Å.

transition state TS-OOH, there is a proton transfer from the O_a atom coordinated to Sn to the O_5 atom of the cluster model, with a calculated activation barrier of 12.6 kcal mol^{-1}. In the resulting product, the O_a atom is more strongly bound to tin and more negatively charged ($q=-0.57$e) than in the Z-HP complex ($q=-0.38$e), while the O_a–O_b and O_b–H_b distances do not change significantly. The reaction is endothermic by 4.2 kcal mol^{-1}.

Once the tin–hydroperoxo intermediate Z-OOH is formed, adsorption of cyclohexanone onto the active site can occur in three ways: 1) interaction of the O_c atom of the carbonyl group with the H_a atom forming quite a strong hydrogen bond (structure R2 in Scheme 3), 2) coordination of the carbonyl group to the Sn atom (shown in structure R3), and 3) interaction of O_c with H_b through another strong hydrogen bond, as shown in structure R4. The calculated CH adsorption energies for these complexes are not too different: −11.3, −10.4, and −9.9 kcal mol^{-1} for R2, R3, and R4, respectively. The complete mechanism for the reaction of R2 is shown in Scheme 4, the optimized geometries of these structures are summarized in Table 3, and the calculated energy profile is depicted in Figure 1b. In the case of R3 it was not possible to localize any transition state converting the reactants complex into a reaction intermediate that could finally yield the ε-caprolactone product. With respect to R4, a reaction mechanism starting from a ketone bound to the H atom of the Sn(OH)$_3$–OOH group (a system equivalent to R4) was investigated by Sever and Root,[6b] and they concluded that the activation barriers involved were so high that it would not occur to any significant extent. The reason for these high activation barriers is that a mechanism starting from this structure is almost equivalent to that obtained in the gas-phase or noncatalyzed process, and therefore we have not investigated this path either.

As shown in Figure 1b and Scheme 4, R2 is converted into the Criegee intermediate CI2 through transition state TS3 with activation energy of 5.9 kcal mol^{-1}. In a concerted manner, the O_a bound to Sn attacks the carbonyl C atom, the CO double bond weakens, and the H_a proton attached to O_5 is transferred to the carbonyl O_c atom. If the optimized geometries of CI2 and the CI structure obtained in the noncatalyzed process are compared, it is found that CI2

Table 3. Optimized values of the most important distances [Å] of the structures involved in mechanism 2. The atom labeling is shown in Scheme 4.

	R2	TS3	CI2	TS4	CI3	TS5	P2
rSn–O_a	1.967	2.051	2.368	2.699	3.237	3.111	3.706
rSn–O_b	2.806	2.853	3.193	2.826	2.346	2.086	1.917
$r$$O_a$–$O_b$	1.449	1.439	1.452	1.453	1.459	1.948	3.269
rC–O_a	3.472	2.181	1.485	1.449	1.442	1.303	1.329
rC–O_c	1.230	1.268	1.374	1.400	1.385	1.322	1.224
$r$$O_c$–$H_a$	1.574	1.145	0.978	0.983	0.979	1.038	1.676
$r$$H_a$–$O_5$	1.010	1.255	1.820	1.800	1.816	1.464	0.998
rSn–O_5	2.185	2.036	1.930	1.937	1.927	1.982	2.218

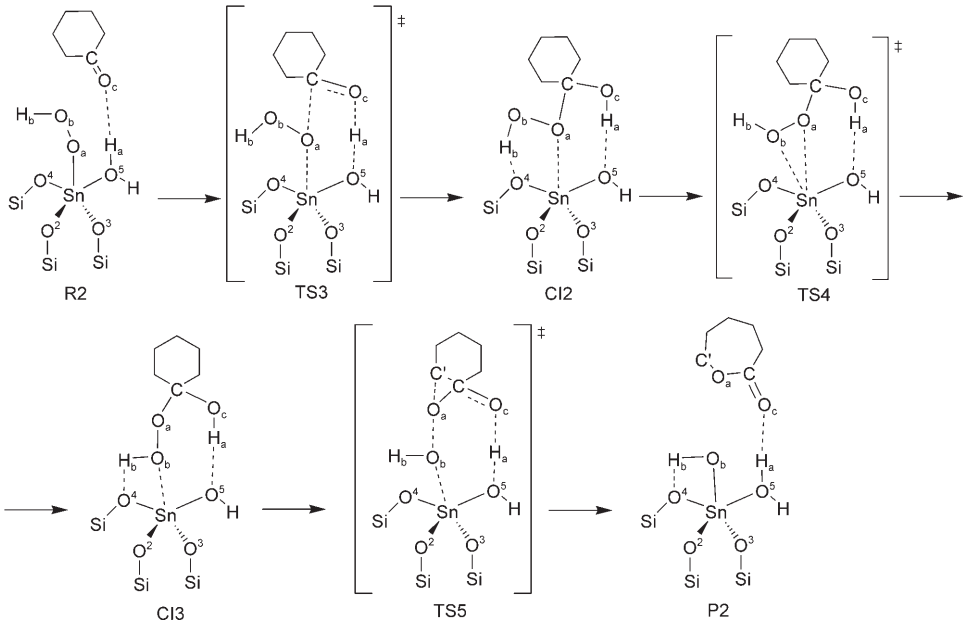

Scheme 4. Structures involved in the Sn-beta-catalyzed Baeyer–Villiger reaction mechanism 2.

can be considered a Z-CI complex in which the organic fragment is bound to the active site through one donor–acceptor Sn–O_a interaction and two quite strong hydrogen bonds (rO_4–H_b = 1.753, rO_5–H_a = 1.820 Å). In a second step, CI2 is converted into a different reaction intermediate, CI3, of similar stability. In structure CI3, the OOH fragment has been reoriented so that the O_b atom is interacting with tin, while the O_a atom is ready to attack the C–C′ bond. The process occurs through transition state TS4 with an activation energy value of only 5.7 kcal mol^{-1}. The Sn–O_a and Sn–O_b distances in TS4 are similar, and the tin atom shows nearly octahedral coordination, this being the reason for the low activation barrier. Finally, in transition state TS5, the O_a–O_b bond is broken, the O_a atom is inserted into the C–C′ bond, and the H_a atom is transferred to O_5, regenerating the carbonyl CO double bond. The reaction product obtained, P2, consists of a ε-caprolactone molecule forming quite a strong hydrogen bond with the water molecule coordinated to the tin active site. The activation energy for the rearrangement step, calculated as the energy difference between TS5 and CI3, is high, at 14.6 kcal mol^{-1}. However, if we take as the origin of energies the Z-HP + CH system (see Figure 1b), the rate-determining step in mechanism 2 would not be the rearrangement of CI3, but the initial formation of the tin hydroperoxo intermediate.

Table 4. Adsorption energy [kcal mol^{-1}], CO bond length [Å], scaled stretching frequency [cm^{-1}],[8] net atomic charge on the carbonyl C atom [e], C–O_a distance [Å], orbital energies [au], and HOMO–LUMO energy gap [eV] of cyclohexanone coordinated to H_2O_2 and forming different adsorption complexes with Sn-beta catalyst.

	E_{ads}	rCO	$\tilde{\nu}_{CO}$	q_{C+}	rC–O_a	E_{HOMO}[a]	E_{LUMO}[b]	ΔE
CH		1.215	1753.8	0.439			−0.013	
R	−7.1	1.223	1722.9	0.460	3.460	−0.246	−0.032	5.82
Z-CH	−9.7	1.230	1694.5	0.506		−0.279[c]	−0.063	5.88
Z-w-CH	−4.9	1.236	1678.3	0.501		−0.271[c]	−0.067	5.55
R1	−8.8 (−14.7)[d]	1.240	1654.0	0.517	2.824	−0.268	−0.056	5.77
R2	−11.3	1.230	1692.2	0.485	3.472	−0.241	−0.042	5.42
R3	−10.4	1.235	1679.6	0.501	3.838	−0.243	−0.069	4.73
R4	−9.9	1.227	1708.6	0.470	3.738	−0.272	−0.047[e]	6.12

[a] Localized on O–O, as depicted in Figure 6. [b] π^*_{CO} of CH. [c] Combination of the p_z orbitals on the O atoms of the cluster. [d] Considering that HP is initially coordinated to the O_5 atom. [e] LUMO+1. The LUMO is the $4\sigma^*_{Sn\text{-}O}$ and lies at −0.051 au.

Although the activation energies for the addition and rearrangement steps of mechanisms 1 and 2 are quite similar, comparison of the calculated energy profiles depicted in Figure 1 shows that while adsorption of the reactants to form R1 is exothermic by 14.1 kcal mol^{-1}, mechanism 2 requires the initial formation of the Z-OOH species with a net energy cost of 7.4 kcal mol^{-1}. Also, in a previous study[4c] we measured the diffuse-reflectance UV-visible spectrum of a sample of Sn-beta zeolite treated with H_2O_2 and we did not observe any band that could be associated with a Sn–OOH species. Therefore, on the basis of energetic considerations and taking into account the available experimental results, it could be concluded that the Sn-beta-catalyzed oxidation of cyclohexanone by H_2O_2 follows mechanism 1.

Cyclohexanone activation: Activation of the CH carbonyl group implies a weakening of the CO double bond, which is reflected in a longer CO bond length, a smaller vibration frequency ($\tilde{\nu}_{CO}$), and a higher positive charge on the carbon atom. These variables, together with calculated adsorption energies, C–O_a distances, and HOMO and LUMO orbital energies of several systems are listed in Table 4. It can be seen that CH is better when activated by Sn-beta instead of by HP in the homogeneous phase, the larger degree of activation being found in structure R1. As previously explained, activation of CH is caused by the donor–acceptor interaction between the HOMO of HP or the catalyst system and the antibonding π^*_{CO} orbital of CH. The strength of this interaction depends on the HOMO–LUMO energy gap (ΔE in Table 4) and on the relative orientation and overlap of the orbitals involved. When the carbonyl group interacts with a proton through a hydrogen bond (like in structures R, R2, and R4) the π^*_{CO} orbital is slightly stabilized, but the decrease in this orbital energy caused by direct coordination of the CO group to the Sn atom is more important. With respect to the HOMO, it is a combination of the lone pairs on the oxygen atoms of the cluster in the case of the Z-CH complex. But in all other structures (R and R1–R4), the HOMO is a combination of the lone pairs on the two oxygen atoms in the O–O fragment, as depicted in Figure 2. The smallest HOMO–LUMO energy gap is obtained for

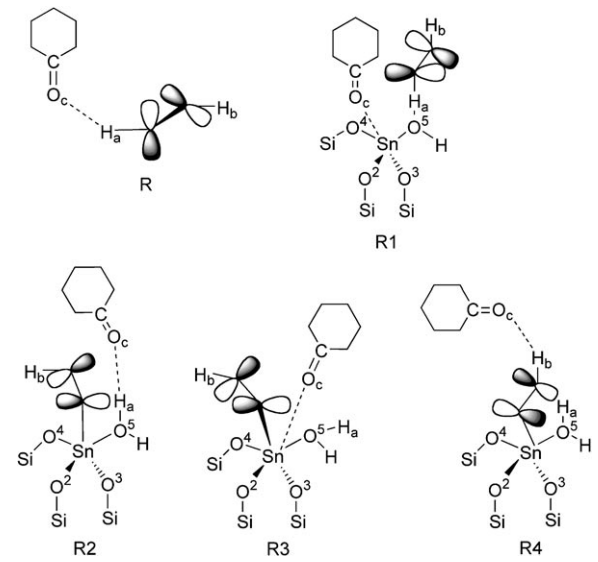

Figure 2. HOMO orientation in the reactant complexes studied in this work.

structure R3, in which CH is coordinated to the Sn atom in the Z-OOH hydroperoxo intermediate. However, the C–O_a distance in this structure is 3.8 Å, and the orbital lobes are orientated in such a way that the HOMO–LUMO overlap is small. Something similar occurs in structures R2 and R4, with large C–O_a distances and a small orbital overlap. On the contrary, in structure R1 the C–O_a distance is as small as 2.8 Å and the orbital lobe located on O_a is directly pointing to the carbonyl group. This orientation allows a good overlap between the HOMO and LUMO orbitals, this being the reason for the larger degree of CH activation obtained in the R1 structure involved in mechanism 1.

Kinetics: The kinetic rate equation for the Baeyer–Villiger oxidation of cyclohexanone by hydrogen peroxide catalyzed by Sn-beta was deduced by considering that the reaction follows mechanism 1, and that the catalytic active site consists of two centers: the tin atom incorporated into the zeolite framework at which cyclohexanone has to be coordinated, and the oxygen atom of the Sn–OH group prone to accepting hydrogen bonding. The kinetic study was performed by applying initial rates methods. In order to check whether the water (WA) and ε-caprolactone (LA) generated during the reaction adsorb onto the active site and thus have to be included in the kinetic rate equation, the inverse of the initial reaction rate was plotted against WA and LA concentrations, as shown in Figure 3. The linear relationship obtained for ε-caprolactone indicates that it can adsorb on one of the centers, the Sn atom. However, as the ε-caprolactone concentration is zero at the beginning of the reaction and we are working with initial rates, its concentration was not included in the kinetic equation. In contrast, water is always present at the beginning of the reaction in considerable amounts and consequently the initial concentration of H_2O was included in the adsorption term of the kinetic equation. It can be seen in Figure 3 that the relationship between the inverse of the initial reaction rate (r^{-1}) and the water concentration is not linear at high water concentrations, indicating that the order of the water concentration in the denominator of the kinetic equation is higher than one. This means that water may compete with cyclohexanone for coordination to the Lewis acid center and with hydrogen peroxide for coordination to the oxygen of the Sn–OH group, and therefore its coordination, without deprotonation, to the first center was also taken into account. From all these considerations the following initial rate equation [Eq. (2)] was derived:

$$r_0 = \frac{k[\mathrm{CH}]_0[\mathrm{HP}]_0}{(1 + K_a[\mathrm{CH}]_0 + K_b[\mathrm{HP}]_0 + K_c[\mathrm{WA}]_0)(1 + K_d[\mathrm{HP}]_0 + K_e[\mathrm{WA}]_0)} \quad (2)$$

in which r_0 = initial reaction rate, $[\mathrm{CH}]_0$ = initial concentration of cyclohexanone, $[\mathrm{HP}]_0$ = initial concentration of hydrogen peroxide, $[\mathrm{WA}]_0$ = initial concentration of water, k = rate constant = $k_0[\mathrm{S}]_0$, K_a = adsorption constant of cyclohexanone at the tin center, K_b = adsorption constant of hydrogen peroxide at the tin center, K_c = adsorption constant of water at the tin center, K_d = adsorption constant of hydrogen peroxide at the oxygen center, and K_e = adsorption constant of water at the oxygen center.

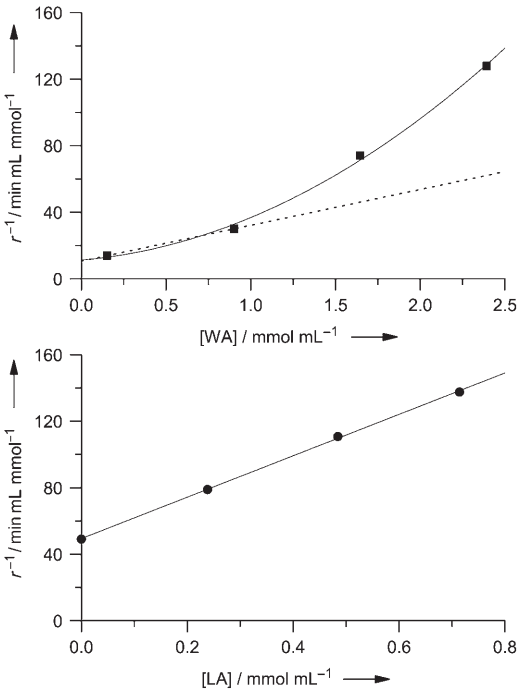

Figure 3. Effect of water (top) and ε-caprolactone (bottom) concentration on the inverse of the initial reaction rate for Sn-beta-catalyzed oxidation of cyclohexanone with hydrogen peroxide.

In order to reduce the number of parameters in Equation (2), the following approximations have been considered: we have assumed that the adsorption constant for H_2O_2 is the same at the two sites ($K_b = K_d$), and that the same applies for the adsorption of water ($K_c = K_e$). Following this, initial reaction rates were calculated by dividing conversion by time at levels of conversion below 10%, and working under the following experimental conditions: A) working with an excess of cyclohexanone and changing the initial concentrations of hydrogen peroxide/water as the limiting reactant, B) studying the effect of water in the presence of the same excess of cyclohexanone as in (A) with hydrogen peroxide as the limiting substrate, and C) changing the initial concentration of cyclohexanone in the presence of an excess of hydrogen peroxide/water. By working under reaction conditions A, B, and C, the kinetic rate and adsorption constants can be calculated as shown in Equations (3)–(6):

$$K_c = \frac{p[\mathrm{HP}]_B}{m} \quad (3)$$

$$K_b = \frac{\frac{q[\mathrm{HP}]_B}{m} - 1}{[\mathrm{HP}]_B} \quad (4)$$

$$k = s(K_b + 3.5K_c)^2[HP]_C \quad (5)$$

$$K_a = \frac{mk[CH]_A - 1}{[CH]_A} \quad (6)$$

in which m, p, and s are the gradients of the slopes in Figures 4, 5, and 6, and q is the y intercept in Figure 5. A good fit of the experimental results to the above equations can be observed in Figures 4–6. The calculated kinetic rate and adsorption constants at different temperatures, as well as the true activation energy and the heats of adsorption for cyclohexanone, H_2O_2, and water are summarized in Table 5. The derivation of Equations (3)–(6) and the experimental data used to obtain Figures 4–6 are available in the Supporting Information.

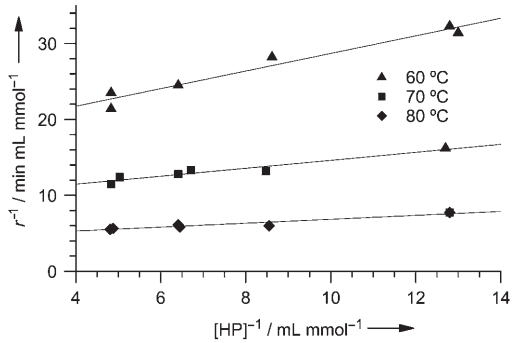

Figure 4. Inverse of the initial reaction rate versus the inverse of the hydrogen peroxide concentration at 60, 70, and 80 °C. Regression lines are as follows: at 60 °C, $y = 1.16x + 17.1$, $R^2 = 0.9567$; at 70 °C, $y = 0.525x + 9.37$, $R^2 = 0.9297$; at 80 °C, $y = 0.258x + 4.27$, $R^2 = 0.9084$.

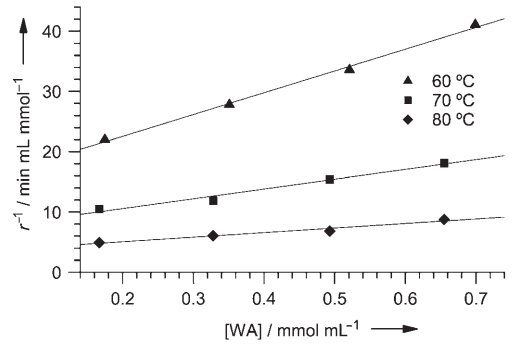

Figure 5. Inverse of the initial reaction rate versus water concentration at 60, 70, and 80 °C. Regression lines are as follows: at 60 °C, $y = 36.2x + 15.3$, $R^2 = 0.9963$; at 70 °C, $y = 16.2x + 7.34$, $R^2 = 0.9774$; at 80 °C, $y = 7.60x + 3.54$, $R^2 = 0.9648$.

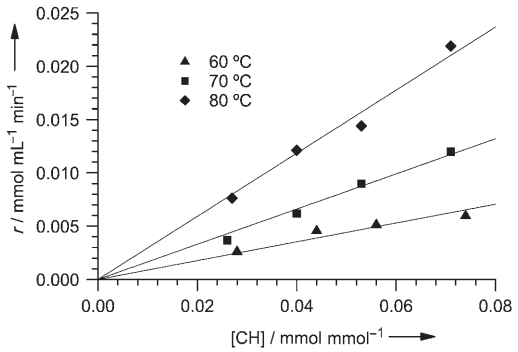

Figure 6. Initial reaction rate versus cyclohexanone concentration at 60, 70, and 80 °C. Regression lines are as follows: at 60 °C, $y = 0.296x$, $R^2 = 0.9753$; at 70 °C, $y = 0.165x$, $R^2 = 0.9821$; at 80 °C, $y = 0.0882x$, $R^2 = 0.8636$.

Table 5. Experimental values of the rate constant k [min^{-1}] and the adsorption constants K_a, K_b, and K_c at the three temperatures [°C] used in the kinetic study, and the activation energy and heats of adsorption [kcal mol^{-1}].

T	k	K_a (CH)	K_b (HP)	K_c (WA)
60	11.7	12.2	2.64	2.96
70	18.7	8.50	2.62	2.72
80	29.9	6.39	2.36	2.59
E_{act}	11.0			
E_{ads}		−7.6	−1.3	−1.6

An activation energy value of 11 kcal mol^{-1} has been obtained experimentally for the Baeyer–Villiger oxidation of cyclohexanone with hydrogen peroxide, a value somewhat lower than the activation energy calculated (14.8 kcal mol^{-1}) for mechanism 1 using cluster B to simulate the catalyst active site, and which corresponds to the energy difference between the transition state for the rearrangement step (TS2) and the reactants complex (R1).

Competitive adsorption on the active sites: The kinetic study shows that WA competes with CH for coordination to the Sn center and with HP for coordination to the O atom of the Sn−OH group, while LA only adsorbs onto the Lewis acid center. The heats of adsorption for those molecules calculated theoretically are given in Table 1. They indicate that WA favorably competes with HP and CH for adsorption on Sn atoms. Thus, as water is always present in excess in the reaction medium, we can assume that one water molecule will permanently be bound to tin during the reaction, and consequently the catalyst active site will be better described by the $(H_3Si)_3Sn(H_2O)OH$ complex than by the $(H_3Si)_3SnOH$ model used before. Therefore, the new cluster denoted as cluster B-w, has been used in this section as a model for the catalyst active site, and the results obtained have been included in Table 1. It was found that coordination of any of the molecules considered to the Sn atom of cluster B-w is more difficult than for cluster B. This can be explained by considering that adsorption of the first WA molecule destabilizes the LUMO of the catalyst, the energy of which rises from −0.064 to −0.046 au, thus making it more inaccessible to the HOMO of the Lewis bases. At the same time, the net atomic charge on O_5 increases from −0.796e in model B to −0.824e in model B-w, facilitating the hydrogen interaction with WA and HP. Thus, adsorption of WA and HP onto O_5 is more exothermic than on Sn when model B-w is used, and the calculated heats of adsorp-

tion for both molecules on O_5 are similar (-14.0 kcal mol^{-1}). In order to check the effect that a molecule of water permanently coordinated to tin has on the reaction path previously obtained, mechanism 1 has been recalculated using cluster B-w as a model for the active site. The optimized Sn–OH_2 distance in the cluster model is 2.303 Å, and it varies between 2.278 and 2.377 Å as the reaction proceeds, indicating that the water molecule is all the time strongly bound to the tin atom. The optimized geometries of all the structures calculated with cluster B-w are equivalent to those obtained with cluster B, and are available in the Supporting Information (Table S7). The energy results are included in brackets in Figure 1a. As previously mentioned, adsorption of HP and CH onto a Sn atom that has a coordinated water molecule is energetically disfavored with respect to the H_2O-free tin center. This destabilization of the reactants complex R1 on model B-w with respect to that obtained with model B causes a decrease in the calculated activation energies for the addition and rearrangement steps of ~2 and 4 kcal mol^{-1}, respectively. The activation barrier for the Baeyer–Villiger reaction calculated as the energy difference between the transition state for the rearrangement step (TS2) and the reactants complex (R1) is 9.0 kcal mol^{-1}, which is in better agreement with the value of 11 kcal mol^{-1} obtained experimentally.

With respect to ε-caprolactone, the heat of adsorption is about 5 kcal mol^{-1} higher than that for cyclohexanone, regardless of the cluster model considered (see Table 1). Interestingly, water interacts more strongly with ε-caprolactone than with cyclohexanone, as can be deduced from the energies of formation of the complexes CH-WA (-5.62 kcal mol^{-1}) and LA-WA (-11.9 kcal mol^{-1}). Taking into account this interaction and using model B-w to simulate the active site, the calculated adsorption energies for cyclohexanone and ε-caprolactone are -9.5 and -9.6 kcal mol^{-1}, respectively. A quantitative comparison between the adsorption energies obtained from the quantum-chemical calculations and from the kinetic study is difficult, due to the errors involved and the various additional stabilizations included in solution. One option could be to calculate the adsorption energy of two molecules at once, as for example in the adsorption of the reactants ($Z+R \rightarrow R1$). In this case, the kinetic estimation for the sum of the adsorption energies of CH and HP is -8.9 kcal mol^{-1}, versus -8.8 kcal mol^{-1} obtained from the theoretical calculations using model B-w to simulate the catalyst active site (see Figure 1).

In summary, it can be concluded that the catalyst active site exists as a $(\equiv SiO)_3Sn(H_2O)OH$ species, with at least one water molecule permanently coordinated to tin, and that adsorption of ε-caprolactone onto tin or adsorption of a water molecule onto either tin or the basic O atom lowers the reaction rate.

Conclusion

The mechanism of the Baeyer–Villiger oxidation of cyclohexanone with hydrogen peroxide catalyzed by Sn-beta zeolite has been theoretically investigated and compared with the gas-phase process. Based on the results obtained, a kinetic model has been proposed and validated with experimental data.

It has been found that a certain degree of flexibility in the framework is needed to allow the interaction between the tin center and the molecules present in the reaction medium to occur, a flexibility which can be provided by Sn–OH defects present in the framework. The theoretical study indicates that the zeolite active site consists of two catalytic centers: the Lewis acidic Sn atom on which the cyclohexanone carbonyl group is activated and an adjacent basic oxygen atom prone to forming hydrogen bonds. Adsorption of hydrogen peroxide onto this second center results in the formation of a complex (R1) in which the orientation of the two reactants is very favorable for the Baeyer–Villiger oxidation. The complete mechanism for the Sn-beta-catalyzed oxidation of CH with HP involves conversion of R1 into a Criegee intermediate, and subsequent rearrangement of this intermediate into ε-caprolactone and a water molecule, with an apparent activation energy no higher than 6 kcal mol^{-1} (mechanism 1). On the other hand, activation of HP through formation of a tin–hydroperoxo species is endothermic by 4 kcal mol^{-1} and requires activation energy of almost 13 kcal mol^{-1}, which makes this mechanism (mechanism 2) less probable.

The kinetic study supports reaction mechanism 1. The relationship between the inverse of the initial reaction rates and the water concentration is linear only at low water concentrations, indicating that water adsorbs onto both the Lewis tin center, competing with CH for this site, and onto the basic O atom to which HP has to coordinate. As water is always present in excess in the reaction medium, its effect on the calculated mechanism has been investigated. The results indicate that the active site could be better described by a $(H_3Si)_3Sn(H_2O)OH$ model, in which a water molecule becomes permanently bound to tin. The activation energy calculated with this model is in agreement with the value obtained from the kinetic study.

Experimental Section

Models and computational methods: Zeolite beta is a large-pore synthetic zeolite with a three-dimensional 12-ring channel system. There are two straight channels in the [100] and [010] directions, and a third sinusoidal channel located parallel to the [001] direction in the A polymorph. These channels intersect, leading to an open-pore structure. The secondary building units consist of 6-, 5-, and 4-membered-ring cages, each of them facing at least one side to a 12-membered-ring channel. Within this crystal structure there are 9 crystallographically different positions, designated as T1 through T9. Zeolite beta crystallizes in a tetragonal $P4_122$ space group with lattice parameters $a=12.661$, $b=12.661$, and $c=26.402$ Å, and has 192 atoms in the conventional unit cell.[9]

In the first step, a theoretical study of the location of Sn in zeolite beta was performed by using atomistic force-field techniques and the GULP code.[10] In order to model realistically the features of the Si→Sn substitution in a solid, a new force field was parameterized to take into account the features of Sn in a zeolite framework. A description of the force field used and the interatomic potential parameters obtained are available in the Supporting Information. In these periodic calculations, one Si atom per cell is substituted by Sn (Si/Sn ratio = 63), and all the atoms of the cell and also the cell parameters are allowed to relax, so that the relevant features of structural flexibility of the solid are reproduced. This study indicates that, from a thermodynamic point of view, only T7, T8, and T9 crystallographic positions of beta zeolite allow the accommodation of one Sn atom per unit cell, the calculated Si→Sn substitution energies being 13.8, 13.6, and 13.5 eV for T7, T8, and T9 positions, respectively. Sn incorporation in the T9 crystallographic position (see Figure 7) causes the displacement of two of the four oxygen atoms bound to Sn towards the inner part of the cavity, resulting in smaller Sn-O-Si angles. These oxygen movements allow the accommodation of the large Sn–O bonds with small variations in the Sn–Si distances, the deformation of which is energetically less favorable.

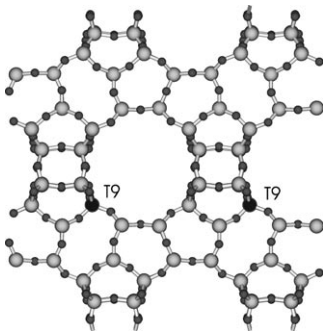

Figure 7. Optimized structure of beta zeolite with Sn (black balls) introduced in the T9 position.

A cluster of atoms was then cut out from the optimized structure of beta zeolite with Sn introduced in the T9 position. It contains the Sn atom, the four oxygen atoms in the first coordination sphere, and the four Si atoms bound to them. The dangling bonds that connected the cluster to the rest of the solid were saturated with H atoms at 1.49 Å from the Si atoms and orientated towards the positions occupied in the crystal by the oxygen atoms in the next coordination sphere. The resulting cluster, $Sn(OSiH_3)_4$, is denoted as model A. In order to check whether defects in the framework may facilitate the reaction, a $Sn(OSiH_3)_3OH$ system (model B) was created by substituting one siloxyl group in cluster A by one hydroxyl group. The coordinates of the organic molecules, the Sn, O, and Si atoms of both clusters and the H of the hydroxyl group in cluster B were completely optimized in all calculations, while the H terminations of the Si atoms were kept fixed at the original positions in the crystal. A third series of calculations was performed in which the H terminations of one siloxyl group in cluster A were also optimized. By doing this, we made sure that the flexibility of this model, denoted as A′, and model B were the same, and consequently that any differences found in the results obtained were caused by the nature of the catalyst and not by the different constraints imposed on the model. Geometry optimizations were performed by using the density functional B3PW91 method,[11] a LANL2DZ effective core potential basis set for Sn,[12] and the standard 6-31G(d,p) basis set[13] for C, O, Si, and H atoms. The nature of every stationary point was characterized by means of frequency calculations and analysis of the vibrational modes, and all calculated energies were corrected for the zero-point vibrational energies (ZPE). Due to the restrictions imposed on the H terminations of the cluster models, some imaginary vibrational modes with frequencies lower than 100 cm^{-1} have sometimes been obtained, but in all cases it has been checked that they are associated with the movement of these H terminations and not with the atoms involved in the reaction path. All DFT calculations were performed by using the Gaussian 98 computer program.[14]

Synthesis of the molecular sieves: Sn-beta was synthesized according to literature procedures.[4c,15] The Sn content (2.0 wt % of SnO_2) was determined by using atomic absorption analysis. The Sn-beta zeolite was calcined at 853 K for 3 h. A high crystallinity of the zeolite was observed by X-ray diffraction (XRD) analysis, and no peaks of SnO_2 were found in the diffractogram. Nitrogen adsorption experiments on the calcined beta samples gave an isotherm very similar to that of pure silica beta with a micropore volume of 0.20–0.21 cm^3g^{-1} and BET surface areas of 450–475 m^2g^{-1}.

General procedure for the Baeyer–Villiger oxidation: Sets of four reactions were carried out on a multibatch high-throughput automatic reactor (for description of the apparatus see reference [16]). Each reaction was carried out in a 1.5 mL glass vial with magnetic stirring. Cyclohexanone, hydrogen peroxide, optionally water, optionally ε-caprolactone, and dioxane were mixed at the concentrations given in the Supporting Information. Then, after reaching the reaction temperature, the catalyst (5 mg) was added and the reaction started. The analysis was performed within 90 s, on a 3 m HP-5 column. This system allowed an analysis to be carried out in each reactor every eight minutes.

Acknowledgements

The authors thank the Comisión Interministerial de Ciencia y Tecnología (CICYT, MAT2003-07945-C02-01) for financing this work and the Universitat de Valencia for computing facilities. M.R. is grateful to the Spanish Ministry of Science and Technology for a "Ramón y Cajal" Fellowship.

[1] a) A. Baeyer, V. Villiger, *Ber. Dtsch. Chem. Ges.* **1899**, *32*, 3625; b) M. Renz, B. Meunier, *Eur. J. Org. Chem.* **1999**, *64*, 737–750; c) G. R. Krow, *Org. React.* **1993**, *43*, 251–798; d) G. Strukul, *Angew. Chem.* **1998**, *110*, 1256–1267; *Angew. Chem. Int. Ed.* **1998**, *37*, 1198–1209.

[2] a) G. Gavagnin, M. Cataldo, F. Pinna, G. Strukul, *Organometallics* **1998**, *17*, 661–667; b) G. Strukul, A. Varagnolo, F. Pinna, *J. Mol. Catal. A* **1997**, *117*, 413–423; c) A. M. F. Phillips, C. Romao, *Eur. J. Org. Chem.* **1999**, *64*, 1767–1770; d) G. J. T. Brink, J. M. Vis, I. W. C. E. Arends, R. A. Sheldon, *J. Org. Chem.* **2001**, *66*, 2429–2433; e) S. E. Jacobson, R. Tang, F. J. Mares, *J. Chem. Soc. Chem. Commun.* **1978**, 888–889.

[3] a) S. E. Jacobson, F. J. Mares, P. M. Zambri, *J. Am. Chem. Soc.* **1979**, *101*, 6938–6946; b) R. T. Taylor, L. A. Flood, *J. Org. Chem.* **1983**, *48*, 5160–5164; c) J. Fischer, W. F. Hölderich, *Appl. Catal. A* **1999**, *180*, 435–443; d) A. Lambert, D. J. Macquarrie, G. Carr, J. H. Clark, *New J. Chem.* **2000**, *24*, 485–488; e) A. Bhaumik, P. Kumar, R. Kumar, *Catal. Lett.* **1996**, *40*, 47–50.

[4] a) A. Corma, L. Nemeth, M. Renz, S. Valencia, *Nature* **2001**, *412*, 423–425; b) A. Corma, M. T. Navarro, L. Nemeth, M. Renz, *Chem. Commun.* **2001**, 2190–2191; c) M. Renz, T. Blasco, A. Corma, V. Fornés, R. Jensen, L. Nemeth, *Chem. Eur. J.* **2002**, *8*, 4708–4717.

[5] a) V. A. Stoute, M. A. Winnik, I. G. Csizmandia, *J. Am. Chem. Soc.* **1974**, *96*, 6388–6393; b) R. Cardenas, R. Cetina, J. Lagúnez-Otero, L. Reyes, *J. Phys. Chem. A* **1997**, *101*, 192–200; c) Y. Okuno, *Chem. Eur. J.* **1997**, *3*, 212–218; d) P. Carlqvist, R. Eklund, T. Brinck, *J. Org. Chem.* **2001**, *66*, 1193–1199.

[6] a) R. R. Sever, T. W. Root, *J. Phys. Chem. B* **2003**, *107*, 10521–10530; b) R. R. Sever, T. W. Root, *J. Phys. Chem. B* **2003**, *107*, 10848–10862.

[7] a) X. Rozanska, R. A. Van Santen, T. Demuth, F. Hutschka, J. Hafner, *J. Phys. Chem. B* **2003**, *107*, 1309–1315; b) M. Boronat, P. M. Viruela, A. Corma, *J. Am. Chem. Soc.* **2004**, *126*, 3300–3309.

[8] A. P. Scott, L. Radom, *J. Phys. Chem.* **1996**, *100*, 16502–16513.

[9] J. M. Newsam, M. M. J. Treacy, W. T. Koetsier, C. B. de Gruyter, *Proc. R. Soc. London Ser. A* **1988**, *420*, 375–405.
[10] J. D. Gale, *J. Chem. Soc. Faraday Trans.* **1997**, *93*, 629–637.
[11] a) A. D. Becke, *J. Chem. Phys.* **1993**, *98*, 5648–5652; b) J. P. Perdew, Y. Wang, *Phys. Rev. B* **1992**, *45*, 13244–13249.
[12] W. R. Wadt, P. J. Hay, *J. Chem. Phys.* **1985**, *82*, 284–298.
[13] P. C. Hariharan, J. A. Pople, *Theor. Chim. Acta* **1973**, *28*, 213–222.
[14] Gaussian 98 (Revision A.7), M. J. Frisch, G. W. Trucks, H. B. Schlegel, G. E. Scuseria, M. A. Robb, J. R. Cheeseman, V. G. Zakrzewski, J. A. Montgomery, Jr., R. E. Stratmann, J. C. Burant, S. Dapprich, J. M. Millam, A. D. Daniels, K. N. Kudin, M. C. Strain, O. Farkas, J. Tomasi, V. Barone, M. Cossi, R. Cammi, B. Mennucci, C. Pomelli, C. Adamo, S. Clifford, J. Ochterski, G. A. Petersson, P. Y. Ayala, Q. Cui, K. Morokuma, D. K. Malick, A. D. Rabuck, K. Raghavachari, J. B. Foresman, J. Cioslowski, J. V. Ortiz, B. B. Stefanov, G. Liu, A. Liashenko, P. Piskorz, I. Komaromi, R. Gomperts, R. L. Martin, D. J. Fox, T. Keith, M. A. Al-Laham, C. Y. Peng, A. Nanayakkara, C. Gonzalez, M. Challacombe, P. M. W. Gill, B. G. Johnson, W. Chen, M. W. Wong, J. L. Andres, M. Head-Gordon, E. S. Replogle, J. A. Pople, Gaussian, Inc., Pittsburgh, PA, **1998**.
[15] S. Valencia, A. Corma (UOP LCC), US 5968473, **1999**; [*Chem. Abstr.* **1999**, *131*, 301204].
[16] A. Corma, J. M. Serra, P. Serna, E. Argente, S. Valero, V. Botti, *J. Catal.* **2005**, *229*, 513–524.

Received: February 21, 2005
Revised: May 5, 2005
Published online: September 15, 2005

